COMPDYN 2011
3rd ECCOMAS Thematic Conference on
Computational Methods in Structural Dynamics and Earthquake Engineering
M. Papadrakakis, M. Fragiadakis, V. Plevris (eds.)
Corfu, Greece, 25-28 May 2011

FULL-WAVEFORM-BASED INVERSION FOR SITE CHARACTERIZATION: THEORY, NUMERICAL SIMULATIONS, AND PHYSICAL EXPERIMENTS

Sezgin Kucukcoban[1] **and Loukas F. Kallivokas**[1]

[1]Department of Civil, Architectural and Environmental Engineering
The University of Texas at Austin
1 University Station, C1748
Austin, TX, 78712, USA
e-mail: {ksezgin,loukas}@mail.utexas.edu

Keywords: Full-waveform-based inversion, Perfectly-matched-layers, Site characterization, Forward transient elastic wave simulation, Mixed FEM.

Abstract. *We discuss recent progress in the full-waveform-based imaging of probed solids/soils, with geotechnical site characterization applications in mind. The primary goal is the reconstruction of the material profile of near-surface, arbitrarily heterogeneous formations using elastic waves as the probing agents.*

The problem requires efficient solutions of the forward wave simulation problem, robust strategies for tackling the inverse imaging problem, and designing of experimental protocols to best harness the limited field data that feed the imaging problem. To address the forward problem, the semi-infinite extent of the probed domains is truncated via the introduction of perfectly-matched-layers (PMLs) at the truncation interfaces. We discuss a new variational hybrid formulation for transient elastic wave simulations in PML-truncated domains that is computationally optimal when compared to competing schemes. We then discuss a full-waveform-based inversion framework driven by PDE-constrained optimization ideas: to address the imaging problem we seek to resolve simultaneously PML-endowed state and adjoint time-dependent BVPs, together with time-independent BV control problems that drive the material updates during inversion iterations. To address solution multiplicity and improve on the robustness of the inversion algorithms we deploy regularization schemes (Tikhonov and Total Variation), continuation schemes (frequency-, grid-, and regularization factor-continuations), and a new search-direction biasing scheme that seems to accelerate algorithmic convergence.

We report satisfactory results with numerical experiments targeting inversion of both smooth and sharp profiles in two dimensions, and also provide examples attesting to the quality and efficiency of the forward wave modeling.

1 INTRODUCTION

Recent advances in both algorithms and computer hardware architecture have renewed hope that problems associated with the non-invasive condition assessment of physical and biological systems are becoming more tractable with present means. The last thirty years have seen various developments aiming at the solution of such mathematically, algorithmically, and computationally challenging inverse problem that arises in various application domains ranging from seismic to medical imaging. The inverse medium problem in the context of geotechnical site characterization, reduces to the reconstruction of the soil's material profile, i.e., of the spatial distribution of the elastic material properties (Lamé parameters $\{\lambda, \mu\}$ or, to an extent, equivalently, of the P- and S-wave velocities, $\{c_p, c_s\}$).

Since the focus is on characterizing near-surface deposits, the truncation of the semi-infinite extent of the physical domain becomes necessary. We, thus, introduce perfectly-matched-layers (PMLs) [1, 2, 3, 4, 5, 6] to convert the semi-infinite physical domain to a finite computational model that mimics the physical behavior of the non-truncated domain. The PML is a truly absorbing condition, capable of handling heterogeneity, unlike any other competing methodology. The PML attenuates propagating waves without reflection from the interface for all non-zero angles-of-incidences and frequencies (Fig. 2(a)). Here, we address the numerical simulation of elastic wave motion in two-dimensional, PML-truncated, arbitrarily heterogeneous elastic media (*forward problem*). Specifically, we discuss a new hybrid, fully symmetric, variational formulation (mixed unsplit-field PML, coupled with a non-mixed approach for the interior domain) for direct transient analysis. The hybrid formulation leads to optimal computational cost and easy modification of existing interior-domain displacement-based codes to accommodate PMLs as a means of domain truncation.

To address the inverse medium problem, we favor a full waveform inversion approach that uses stress waves for interrogation, and is driven by the measurements collected directly in the time-domain at receivers on the soil's surface, as schematically shown in Figs. 1(a) and 1(b). We

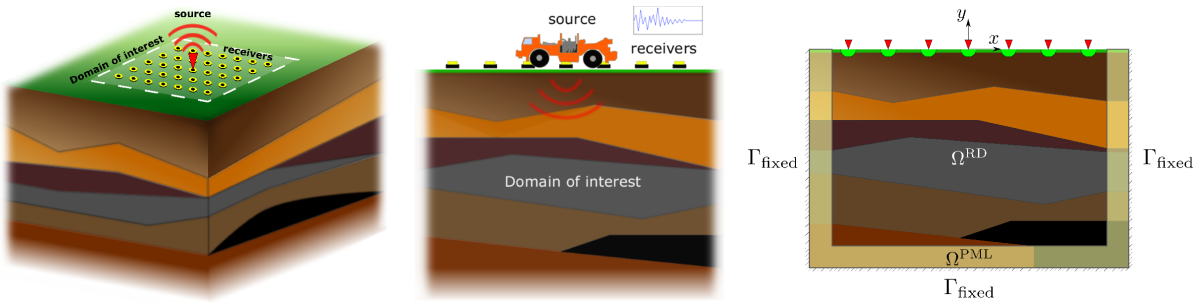

(a) (b) (c)

Figure 1: Problem definition: (a) interrogation of a heterogeneous semi-infinite domain by an active source; (b) a 2D cross-section of the domain showing one source and multiple receivers; and (c) computational model truncated from the semi-infinite medium via the introduction of PMLs

cast the profile reconstruction problem as a PDE-constrained least-squares misfit optimization problem [7, 8] , and then recast it with the aid of a Lagrangian, whereby the misfit functional is augmented with the side-imposition of the PML-endowed PDEs, initial, and boundary conditions via Lagrange multipliers. To enforce the stationarity of the Lagrangian, we derive next the first-order optimality conditions. Upon discretization, the coupled system results in a classic KKT (Karush-Kuhn-Tucker) system. To solve, we pursue a *reduced-space approach* in which

the coupled system of PDEs are solved in the reduced space of the control variables –the Lamé parameters. To alleviate the difficulties associated with solution multiplicity, we explore both Tikhonov (TN) and Total Variation (TV) regularization schemes. To aid the inversion process in reconstructing high-quality material profiles, we deploy regularization factor continuation and source-frequency continuation schemes. We present examples involving layered systems and smoothly-varying profiles, as well as layered systems containing inclusions to demonstrate the performance of the proposed inversion approach and associated algorithms.

2 2D ELASTIC WAVE HYBRID MODELING

First, the equilibrium equation and the kinematic condition combined with the constitutive law, are Fourier-transformed into the frequency-domain, to obtain

$$\mathbf{div}\,\hat{\mathcal{S}}^T + \hat{\mathbf{f}} = -\omega^2\rho\hat{\mathbf{u}}, \qquad \mathcal{D}:\hat{\mathcal{S}} = \frac{1}{2}\left[\nabla\hat{\mathbf{u}} + (\nabla\hat{\mathbf{u}})^T\right], \tag{1}$$

where $\mathcal{S}$, $\mathcal{E}$, and $\mathcal{D}$ are the stress, strain, and compliance tensors, respectively; ρ is the density of the elastic medium, $\mathbf{u}$ is the displacement vector, $\mathbf{f}$ is the load vector, and (:) denotes tensor inner product. Next, we introduce the coordinate-stretched form for each coordinate:

$$\begin{aligned} \tilde{s} &= \int_0^s \varepsilon_s(s')ds', \qquad \varepsilon_s(s,\omega) = \alpha_s(s) + \frac{\beta_s(s)}{i\omega}, \\ \frac{d}{d\tilde{s}} &= \frac{1}{\varepsilon_s(s,\omega)}\frac{d}{ds}, \qquad s = x, y, \end{aligned} \tag{2}$$

where ω denotes circular frequency, ε_s is a complex stretching function in the direction of coordinate s, and α_s and β_s denote scaling and attenuation functions, respectively. As the names imply, α_s "stretches" or scales s, whereas β_s is responsible for the amplitude decay of the propagating wave once it enters the PML.

The stretching is applied by replacing x and y in (1) with the stretched coordinates $\tilde{x}$ and $\tilde{y}$. Making use of (2), (1) can be written in terms of the non-stretched coordinates, and then, inverted back into the time domain to obtain a mixed unsplit-field PML formulation:

$$\mathbf{div}\left(\dot{\mathbf{S}}^T\tilde{\Lambda}_e + \mathbf{S}^T\tilde{\Lambda}_p\right) + a\mathbf{f} = \rho\left(a\ddot{\mathbf{u}} + b\dot{\mathbf{u}} + c\mathbf{u}\right), \tag{3a}$$

$$\mathcal{D}:\left(a\ddot{\mathbf{S}} + b\dot{\mathbf{S}} + c\mathbf{S}\right) = \frac{1}{2}\left[(\nabla\dot{\mathbf{u}})\tilde{\Lambda}_e + \tilde{\Lambda}_e(\nabla\dot{\mathbf{u}})^T + (\nabla\mathbf{u})\tilde{\Lambda}_p + \tilde{\Lambda}_p(\nabla\mathbf{u})^T\right], \tag{3b}$$

in which $a = \alpha_x\alpha_y$, $b = \alpha_x\beta_y + \alpha_y\beta_x$, $c = \beta_x\beta_y$, and $\tilde{\Lambda}_e$ and $\tilde{\Lambda}_p$ define the diagonal stretch tensors where the subscripts "e" and "p" refer to attenuation functions associated with evanescent and propagating waves, respectively. In the regular domain, $\tilde{\Lambda}_e$ reduces to the identity tensor, whereas $\tilde{\Lambda}_p$ vanishes identically. In (3), we introduce an auxiliary variable $\mathbf{S}(\mathbf{x},t)$, which physically represent stress memories or histories, defined as

$$\mathbf{S}(\mathbf{x},t) = \int_0^t \mathcal{S}(\mathbf{x},\tau)d\tau \qquad \text{and consequently, } \dot{\mathbf{S}}(\mathbf{x},t) = \mathcal{S}(\mathbf{x},t). \tag{4}$$

Owing to the complexity of (3), one could not conceivably reduce (3) to a single unknown field, as it is routinely done in displacement-based interior elastodynamics problems, without increasing the temporal complexity. Here, we propose a hybrid approach, whereby we retain a displacement-based interior problem and couple it with the mixed unsplit PML. Thus, the

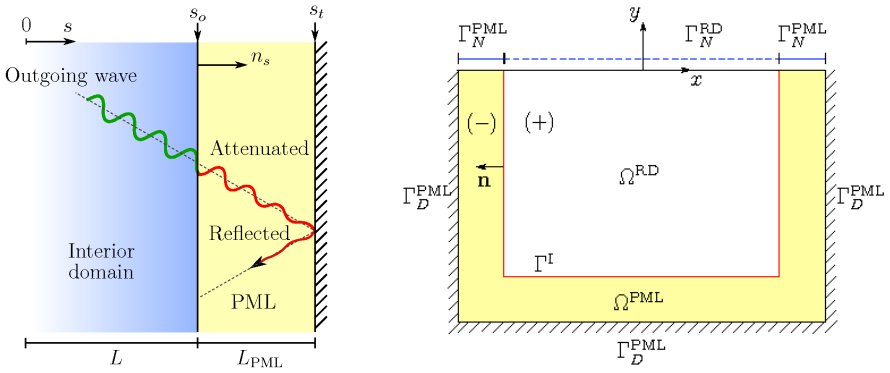

Figure 2: PML-truncated semi-infinite domains in 1D and 2D

wave motion in a PML-truncated domain (Figure 2(b)) over a time interval of interest, $(0, T]$ is governed by the hybrid system of equations:

$$\mathbf{div}\left\{\mu\left[\nabla\mathbf{u}+(\nabla\mathbf{u})^T\right]+\lambda(\operatorname{div}\mathbf{u})\mathcal{I}\right\}+\mathbf{f}=\rho\ddot{\mathbf{u}} \qquad \text{in } \Omega^{\text{RD}}, \tag{5a}$$

$$\mathbf{div}\left(\dot{\mathbf{S}}^T\tilde{\Lambda}_e+\mathbf{S}^T\tilde{\Lambda}_p\right)=\rho\left(a\ddot{\mathbf{u}}+b\dot{\mathbf{u}}+c\mathbf{u}\right) \qquad \text{in } \Omega^{\text{PML}}, \tag{5b}$$

$$\mathcal{D}:\left(a\ddot{\mathbf{S}}+b\dot{\mathbf{S}}+c\mathbf{S}\right)=\frac{1}{2}\left[(\nabla\dot{\mathbf{u}})\tilde{\Lambda}_e+\tilde{\Lambda}_e(\nabla\dot{\mathbf{u}})^T+(\nabla\mathbf{u})\tilde{\Lambda}_p+\tilde{\Lambda}_p(\nabla\mathbf{u})^T\right] \qquad \text{in } \Omega^{\text{PML}}, \tag{5c}$$

subject to silent initial, and the following boundary and interface conditions:

$$\left\{\mu\left[\nabla\mathbf{u}+(\nabla\mathbf{u})^T\right]+\lambda(\operatorname{div}\mathbf{u})\mathcal{I}\right\}\mathbf{n}=\boldsymbol{g}_n \qquad \text{on } \Gamma_N^{\text{RD}}, \tag{6a}$$

$$(\dot{\mathbf{S}}^T\tilde{\Lambda}_e+\mathbf{S}^T\tilde{\Lambda}_p)\mathbf{n}=\mathbf{0} \qquad \text{on } \Gamma_N^{\text{PML}}, \tag{6b}$$

$$\mathbf{u}=\mathbf{0} \qquad \text{on } \Gamma_D^{\text{PML}}, \tag{6c}$$

$$\mathbf{u}^+=\mathbf{u}^- \qquad \text{on } \Gamma^{\text{I}}, \tag{6d}$$

$$\left\{\mu\left[\nabla\mathbf{u}+(\nabla\mathbf{u})^T\right]+\lambda(\operatorname{div}\mathbf{u})\mathcal{I}\right\}\mathbf{n}=-(\dot{\mathbf{S}}^T\tilde{\Lambda}_e+\mathbf{S}^T\tilde{\Lambda}_p)\mathbf{n} \qquad \text{on } \Gamma^{\text{I}}, \tag{6e}$$

where $\boldsymbol{g}_n$ denotes prescribed tractions. Note that the hybrid approach couples two initially-uncoupled sets of governing equations via the continuity of displacements and tractions at the interface.

We seek next the weak form, in the Galerkin sense, corresponding to the strong form (Eq. 5). We take inner products of (5) with test functions $\mathbf{w}_1(\mathbf{x})$, $\mathbf{w}_2(\mathbf{x})$, and $\mathbf{T}(\mathbf{x})$, and then integrate over Ω^{RD}, Ω^{PML}, and Ω^{PML}, respectively, where the integration by parts is applied to the equilibrium equations (5a) and (5b). By adding the equilibrium equations, the weak form of (5) can be cast as:

$$\begin{aligned}\int_{\Omega^{\text{RD}}}\nabla\mathbf{w}_1:\left\{\mu\left[\nabla\mathbf{u}+(\nabla\mathbf{u})^T\right]+\lambda(\operatorname{div}\mathbf{u})\mathcal{I}\right\}\,\mathrm{d}\Omega+\int_{\Omega^{\text{PML}}}\nabla\mathbf{w}_2:\left(\dot{\mathbf{S}}^T\tilde{\Lambda}_e+\mathbf{S}^T\tilde{\Lambda}_p\right)\,\mathrm{d}\Omega\\ +\int_{\Omega^{\text{RD}}}\mathbf{w}_1\cdot\rho\ddot{\mathbf{u}}\,\mathrm{d}\Omega+\int_{\Omega^{\text{PML}}}\mathbf{w}_2\cdot\rho\left(a\ddot{\mathbf{u}}+b\dot{\mathbf{u}}+c\mathbf{u}\right)\,\mathrm{d}\Omega\\ =\int_{\Gamma_N^{\text{RD}}}\mathbf{w}_1\cdot\boldsymbol{g}_n\,\mathrm{d}\Gamma+\int_{\Omega^{\text{RD}}}\mathbf{w}_1\cdot\mathbf{f}\,\mathrm{d}\Omega,\end{aligned} \tag{7a}$$

$$\int_{\Omega^{\mathrm{PML}}} \mathbf{T} : \left[\mathcal{D} : \left(a\ddot{\mathbf{S}} + b\dot{\mathbf{S}} + c\mathbf{S}\right)\right] \,\mathrm{d}\Omega$$
$$= \frac{1}{2}\int_{\Omega^{\mathrm{PML}}} \mathbf{T} : \left[(\nabla\dot{\mathbf{u}})\tilde{\Lambda}_e + \tilde{\Lambda}_e(\nabla\dot{\mathbf{u}})^T + (\nabla\mathbf{u})\tilde{\Lambda}_p + \tilde{\Lambda}_p(\nabla\mathbf{u})^T\right] \,\mathrm{d}\Omega. \quad (7b)$$

For the mixed finite element implementation of the weak form, both $\mathbf{u}(\mathbf{x},t)$ and $\mathbf{S}(\mathbf{x},t)$ are treated as independent variables that need to be approximated separately now only within the PML domain. Let the basis functions be denoted by $\mathbf{\Phi}$ and $\mathbf{\Psi}$. The trial functions ($\mathbf{u}$, $\mathbf{S}$) and the test functions ($\mathbf{w}$, $\mathbf{T}$) are spatially discretized as

$$\begin{aligned}
u_x(\mathbf{x},t) &\cong \mathbf{\Phi}^T(\mathbf{x})\mathbf{u}_x(t), & u_y(\mathbf{x},t) &\cong \mathbf{\Phi}^T(\mathbf{x})\mathbf{u}_y(t) & & \\
S_{xx}(\mathbf{x},t) &\cong \mathbf{\Psi}^T(\mathbf{x})\mathbf{S}_{xx}(t), & S_{yy}(\mathbf{x},t) &\cong \mathbf{\Psi}^T(\mathbf{x})\mathbf{S}_{yy}(t), & S_{xy}(\mathbf{x},t) &\cong \mathbf{\Psi}^T(\mathbf{x})\mathbf{S}_{xy}(t), \\
w_x(\mathbf{x}) &\cong \mathbf{w}_x^T\mathbf{\Phi}(\mathbf{x}), & w_y(\mathbf{x}) &\cong \mathbf{w}_y^T\mathbf{\Phi}(\mathbf{x}), & & \\
T_{xx}(\mathbf{x}) &\cong \mathbf{T}_{xx}^T\mathbf{\Psi}(\mathbf{x}), & T_{yy}(\mathbf{x}) &\cong \mathbf{T}_{yy}^T\mathbf{\Psi}(\mathbf{x}), & T_{xy}(\mathbf{x}) &\cong \mathbf{T}_{xy}^T\mathbf{\Psi}(\mathbf{x}).
\end{aligned}$$

We, subsequently, obtain the *semi-discrete form* that is second-order in time and is resolved by the classical Newmark-β scheme. We note the resulting matrices are *symmetric*, and that their size is substantially smaller (up to 60% reduction in total number of unknowns in two dimensions) than that required by fully-mixed formulations (split- or unsplit-field), since the interior elastodynamics problem remains purely displacement-based.

To test the accuracy and efficiency of the hybrid formulation, we present two numerical experiments: a homogeneous semi-infinite domain (Fig. 3(a)), and a horizontally-layered medium (Fig. 3(d)). We use a Ricker pulse time signal with a central frequency $f_r = 15$ Hz as: (a) an explosive source placed at the center of the homogeneous domain, and (b) a surface stress load over a region ($-1\mathrm{m} \leq x \leq 1\mathrm{m}$) of the heterogeneous domain. The efficacy and quality of the PML is nicely corroborated by Fig. 3, which shows no discernible reflections from the PML interfaces, nor any residual reflections from the fixed external boundaries, even in the presence of heterogeneity. The various error metrics shown in Fig. 4 that include the domain energy decay, global and point-wise time-dependent norms, and a long-time stability run, all attest to the forward problem's performance.

3 THE INVERSE MEDIUM PROBLEM

We formulate the inverse problem initially as a PDE-constrained least-squares misfit minimization problem (à la [7, 8]), where the misfit is defined as the difference between the measured response ($\mathbf{u}_m$) at the receivers and a computed response ($\mathbf{u}$) that is obtained using trial distributions of the material parameters. The misfit least-squares minimization can be cast as

$$\mathcal{F} := \frac{1}{2}\sum_{j=1}^{N_r}\int_0^T\int_{\Gamma_m} (\mathbf{u}-\mathbf{u}_m)^2\ \delta(\mathbf{x}-\mathbf{x}_j)\,\mathrm{d}\Gamma\,\mathrm{d}t + \mathcal{R}(\lambda,\mu), \quad (9)$$

and is subject to the physics of the problem, as expressed by the forward problem statement shown in the preceding section. In the above, $\mathcal{F}$ denotes the objective functional, Γ_m denotes the part of the surface Γ_N^{RD} occupied by measuring stations, N_r denotes the total number of receivers on the surface, and $\mathcal{R}$ has been introduced to alleviate the solution multiplicity. We explore both TN and TV regularization schemes.

We cast the PDE-constrained inverse medium problem (9) with the aid of a Lagrangian $\mathcal{L}$, whereby the misfit functional $\mathcal{F}$ is augmented with the side-imposition of the governing PDEs

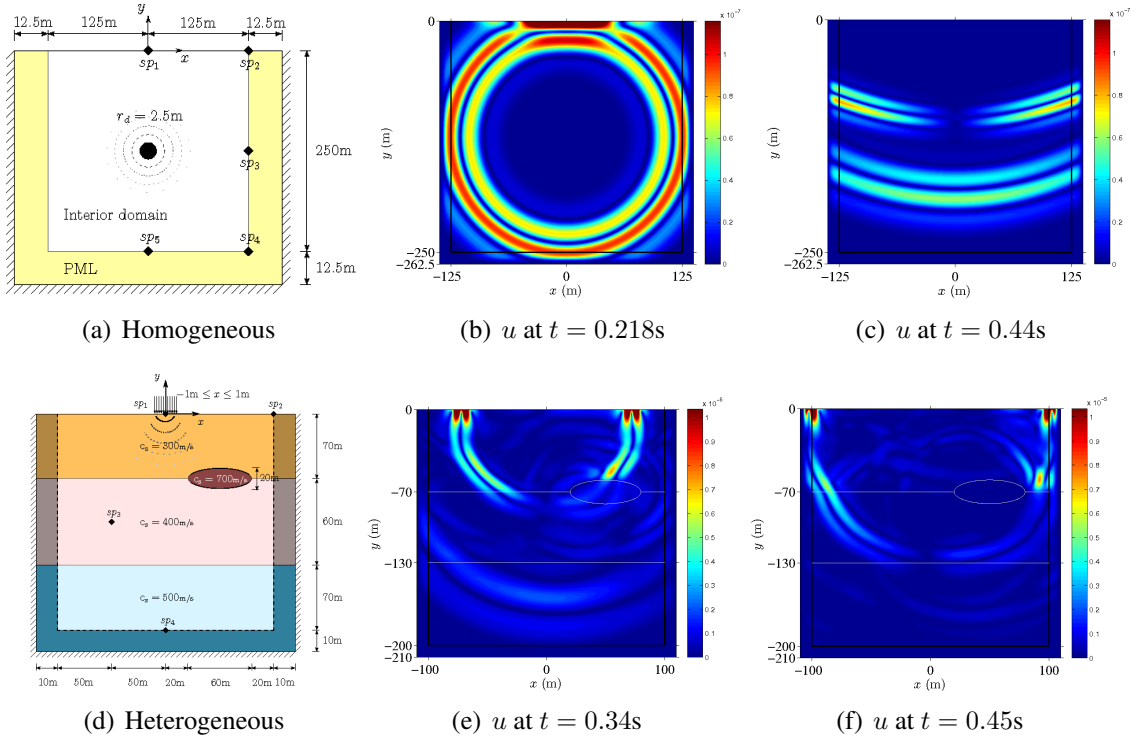

(a) Homogeneous (b) u at $t = 0.218$s (c) u at $t = 0.44$s

(d) Heterogeneous (e) u at $t = 0.34$s (f) u at $t = 0.45$s

Figure 3: PML-truncated medium in two dimensions

and boundary conditions via Lagrange multipliers, per:

$$
\begin{aligned}
&\mathcal{L}(\mathbf{u}, \mathbf{S}, \boldsymbol{\theta_{u1}}, \boldsymbol{\theta_{u2}}, \boldsymbol{\theta_s}, \boldsymbol{\theta_{b1}}, \boldsymbol{\theta_{b2}}, \lambda, \mu) \\
&= \frac{1}{2} \sum_{j=1}^{N_r} \int_0^T \int_{\Gamma_m} (\mathbf{u} - \mathbf{u}_m) \cdot (\mathbf{u} - \mathbf{u}_m)\ \delta(\mathbf{x} - \mathbf{x}_j)\, \mathrm{d}\Gamma \mathrm{d}t \ + \ \mathcal{R}(\lambda, \mu) \\
&+ \int_{\Omega^{\mathrm{RD}}} \int_0^T \boldsymbol{\theta_{u1}} \cdot \left[\mathbf{div} \left\{ \mu \left[\nabla \mathbf{u} + (\nabla \mathbf{u})^T \right] + \lambda (\mathrm{div}\, \mathbf{u}) \mathcal{I} \right\} + \mathbf{f} - \rho \ddot{\mathbf{u}} \right] \mathrm{d}t\, \mathrm{d}\Omega \\
&+ \int_{\Omega^{\mathrm{PML}}} \int_0^T \boldsymbol{\theta_{u2}} \cdot \left[\mathbf{div} \left(\dot{\mathbf{S}}^T \tilde{\Lambda}_e + \mathbf{S}^T \tilde{\Lambda}_p \right) - \rho \left(a \ddot{\mathbf{u}} + b \dot{\mathbf{u}} + c \mathbf{u} \right) \right] \mathrm{d}t\, \mathrm{d}\Omega \\
&+ \int_{\Omega^{\mathrm{PML}}} \int_0^T \boldsymbol{\theta_s} : \left\{ \mathcal{D} : \left(a \ddot{\mathbf{S}} + b \dot{\mathbf{S}} + c \mathbf{S} \right) - \frac{1}{2} \left[(\nabla \dot{\mathbf{u}}) \tilde{\Lambda}_e + \tilde{\Lambda}_e (\nabla \dot{\mathbf{u}})^T + (\nabla \mathbf{u}) \tilde{\Lambda}_p + \tilde{\Lambda}_p (\nabla \mathbf{u})^T \right] \right\} \mathrm{d}t\, \mathrm{d}\Omega \\
&+ \int_{\Gamma_N^{\mathrm{RD}}} \int_0^T \boldsymbol{\theta_{b1}} \cdot \left\{ \left(\mu \left[\nabla \mathbf{u} + (\nabla \mathbf{u})^T \right] + \lambda (\mathrm{div}\, \mathbf{u}) \mathcal{I} \right) \mathbf{n} - \boldsymbol{g}_n \right\} \mathrm{d}t\, \mathrm{d}\Gamma \\
&+ \int_{\Gamma_N^{\mathrm{PML}}} \int_0^T \boldsymbol{\theta_{b2}} \cdot \left[\left(\dot{\mathbf{S}}^T \tilde{\Lambda}_e + \mathbf{S}^T \tilde{\Lambda}_p \right) \mathbf{n} \right] \mathrm{d}t\, \mathrm{d}\Gamma. \qquad (10)
\end{aligned}
$$

In the above and in the parlance customarily used for such problems, $\{\mathbf{u},\ \mathbf{S}\}$ are the *state variables* (s), $\{\boldsymbol{\theta_{u1}},\ \boldsymbol{\theta_{u2}},\ \boldsymbol{\theta_s},\ \boldsymbol{\theta_{b1}},\ \boldsymbol{\theta_{b2}}\}$ are the Lagrange multipliers or *adjoint variables* (m), and $\{\lambda,\ \mu\}$ are the *control variables* (c). We seek to satisfy stationarity of $\mathcal{L}$ by requiring that the first variations of $\mathcal{L}$ vanish.

3.1 The 1st optimality condition (State problem)

The variation of $\mathcal{L}$ with respect to the Lagrange multipliers must vanish; accordingly $\delta_{\mathrm{m}}\mathcal{L} = 0$. There results the *state (or forward) problem*, identical to the IBVP given by (5-6).

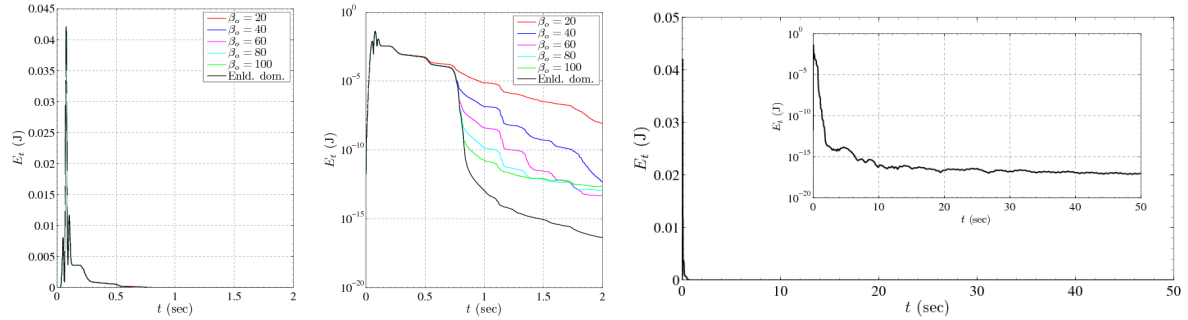

(a) Energy decay (std) (b) Energy decay (log) (c) Long-time stability

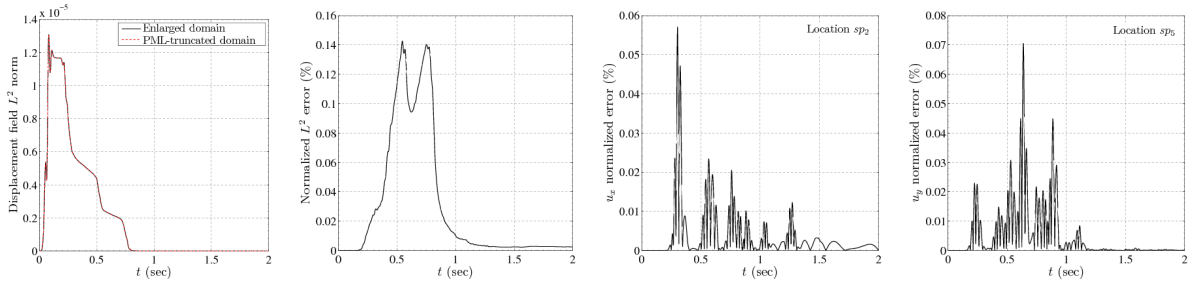

(d) Displacement norm (e) Relative error $e(t)$ (f) $e(t)$ for u_x at sp_2 (g) $e(t)$ for u_y at sp_5

Figure 4: Error metrics for homogeneous domain

3.2 The 2nd optimality condition (Adjoint problem)

Similarly, we enforce the vanishing of the variation of $\mathcal{L}$ with respect to the state variables, that is $\delta_{\mathrm{s}}\mathcal{L} = 0$. There results the following *adjoint problem*:

$$
\begin{aligned}
&\mathbf{div}\left[\mu(\nabla\boldsymbol{\theta_{u1}} + \nabla\boldsymbol{\theta_{u1}}^T) + \lambda\ \mathrm{div}\,\boldsymbol{\theta_{u1}}\,\mathcal{I}\right] = \rho\ddot{\boldsymbol{\theta}}_{\boldsymbol{u1}} && \text{in } \Omega^{\mathrm{RD}},\\
&\mathbf{div}\left(-\dot{\boldsymbol{\theta}}_{\boldsymbol{s}}\tilde{\Lambda}_e + \boldsymbol{\theta_s}\tilde{\Lambda}_p\right) = \rho\left(a\ddot{\boldsymbol{\theta}}_{\boldsymbol{u2}} - b\dot{\boldsymbol{\theta}}_{\boldsymbol{u2}} + c\boldsymbol{\theta_{u2}}\right) && \text{in } \Omega^{\mathrm{PML}},\\
&\mathcal{D}:\left(a\ddot{\boldsymbol{\theta}}_{\boldsymbol{s}} - b\dot{\boldsymbol{\theta}}_{\boldsymbol{s}} + c\boldsymbol{\theta_s}\right) = \tilde{\Lambda}_p\left(\nabla\boldsymbol{\theta_{u2}}\right)^T - \tilde{\Lambda}_e\left(\nabla\dot{\boldsymbol{\theta}}_{\boldsymbol{u2}}\right)^T && \text{in } \Omega^{\mathrm{PML}},
\end{aligned}
$$

subject to

$$
\begin{aligned}
&\left\{\mu(\nabla\boldsymbol{\theta_{u1}} + \nabla\boldsymbol{\theta_{u1}}^T) + \lambda\ \mathrm{div}\,\boldsymbol{\theta_{u1}}\,\mathcal{I}\right\}\mathbf{n} = \sum_{j=1}^{N_r}(\mathbf{u} - \mathbf{u}_m) && \text{on } \Gamma_m,\\
&\left(-\dot{\boldsymbol{\theta}}_{\boldsymbol{s}}\tilde{\Lambda}_e + \boldsymbol{\theta_s}\tilde{\Lambda}_p\right)\mathbf{n} = \mathbf{0} && \text{on } \Gamma_N^{\mathrm{PML}},\\
&\boldsymbol{\theta_{u2}} = \mathbf{0} && \text{on } \Gamma_D^{\mathrm{PML}},\\
&\boldsymbol{\theta_{u1}} = \boldsymbol{\theta_{u2}} && \text{on } \Gamma^{\mathrm{I}},\\
&\left\{2\mu\,\nabla\boldsymbol{\theta}_{\boldsymbol{u1}}^{sym} + \lambda\ \mathrm{div}\,\boldsymbol{\theta_{u1}}\,\mathcal{I}\right\}\mathbf{n} = \left(\dot{\boldsymbol{\theta}}_{\boldsymbol{s}}\tilde{\Lambda}_e - \boldsymbol{\theta_s}\tilde{\Lambda}_p\right)\mathbf{n} && \text{on } \Gamma^{\mathrm{I}},\\
&\boldsymbol{\theta_{u1}}(\mathbf{x},T) = \mathbf{0}, \qquad \dot{\boldsymbol{\theta}}_{\boldsymbol{u1}}(\mathbf{x},T) = \mathbf{0} && \text{in } \Omega^{\mathrm{RD}},\\
&\boldsymbol{\theta_{u2}}(\mathbf{x},T) = \mathbf{0}, \qquad \dot{\boldsymbol{\theta}}_{\boldsymbol{u2}}(\mathbf{x},T) = \mathbf{0} && \text{in } \Omega^{\mathrm{PML}},\\
&\boldsymbol{\theta_s}(\mathbf{x},T) = \mathbf{0}, \qquad \dot{\boldsymbol{\theta}}_{\boldsymbol{s}}(\mathbf{x},T) = \mathbf{0} && \text{in } \Omega^{\mathrm{PML}}.
\end{aligned}
$$

The adjoint problem is a *final-value* problem (requires reverse marching along the time line) and is driven by the misfit between the computed and observed responses at measuring stations. We

note that the operators implicated in the adjoint PDEs are identical to the state operators, modulo the sign reversal for those terms implicating first-order time derivatives. By construction, the adjoint equations are also hybrid and PML-endowed, with $(\boldsymbol{\theta}_{\boldsymbol{u1}}, \boldsymbol{\theta}_{\boldsymbol{u2}})$ and $\boldsymbol{\theta}_{\boldsymbol{s}}$ playing a role analogous to $\mathbf{u}$ and $\mathbf{S}$ of the state problem, respectively.

3.3 The 3rd optimality condition (Control problem)

Lastly, we impose $\delta_\lambda \mathcal{L} = 0$ and $\delta_\mu \mathcal{L} = 0$. The variations result in the following two boundary-value control problems:
λ-control problem:

$$-R_\lambda \Delta\lambda - \int_0^T (\operatorname{div} \boldsymbol{\theta}_{\boldsymbol{u1}})(\operatorname{div} \mathbf{u}) \,\mathrm{dt} = 0 \qquad \text{in } \Omega^{\mathrm{RD}}, \tag{13a}$$

$$\int_{\Gamma_N^{\mathrm{RD}}} \nabla\lambda \cdot \mathbf{n} \,\mathrm{d}\Gamma = 0 \qquad \text{on } \Gamma_N^{\mathrm{RD}}. \tag{13b}$$

μ-control problem:

$$-R_\mu \Delta\mu - \int_0^T \nabla\boldsymbol{\theta}_{\boldsymbol{u1}} : 2\nabla \mathbf{u}^{sym} \,\mathrm{dt} = 0 \qquad \text{in } \Omega^{\mathrm{RD}}, \tag{14a}$$

$$\int_{\Gamma_N^{\mathrm{RD}}} \nabla\mu \cdot \mathbf{n} \,\mathrm{d}\Gamma = 0 \qquad \text{on } \Gamma_N^{\mathrm{RD}}. \tag{14b}$$

In writing (13) and (14), we adopted the TN scheme for regularizing the solutions. If the TV regularization were to be used instead, the first terms in (13a) and (14a) are modified, and the control problems now read

$$-R_\lambda \,\nabla \cdot \left[(\nabla\lambda \cdot \nabla\lambda + \epsilon)^{-\frac{1}{2}} \,\nabla\lambda \right] - \int_0^T (\operatorname{div} \boldsymbol{\theta}_{\boldsymbol{u1}})(\operatorname{div} \mathbf{u}) \,\mathrm{dt} = 0 \qquad \text{in } \Omega^{\mathrm{RD}}, \tag{15}$$

$$-R_\mu \,\nabla \cdot \left[(\nabla\mu \cdot \nabla\mu + \epsilon)^{-\frac{1}{2}} \,\nabla\mu \right] - \int_0^T \nabla\boldsymbol{\theta}_{\boldsymbol{u1}} : \left(\nabla\mathbf{u} + \nabla\mathbf{u}^T \right) \,\mathrm{dt} = 0 \qquad \text{in } \Omega^{\mathrm{RD}}. \tag{16}$$

We remark that the TV scheme leads to a nonlinear operator in the control equations, as opposed to the Laplacian operator that results when TN regularization is used.

4 THE INVERSION PROCESS

To satisfy the stationarity of $\mathcal{L}$, all three problems must be solved. However, the simultaneous solution of the resulting KKT system using a *full-space method* is computationally expensive. Alternatively, a *reduced-space method*, in which the coupled system of PDEs are solved in the reduced space of the control variables, is preferable [7, 8]. The procedure is iterative: we start with an assumed initial spatial distribution of the control parameters (λ and μ) and solve the state problem. Then, we solve the adjoint problem. By doing so, we satisfy the first and second optimality conditions, and we iteratively update the control parameters using a conjugate gradient method with inexact line search so that the misfit reduces to a preset tolerance, thereby allowing the third optimality condition to be satisfied. We bring in two remedies that aid the inversion process in reconstructing high-quality material profiles: (a) a regularization factor continuation scheme to penalize high-frequency material oscillations during the early inversion stages, (b) a source-frequency continuation scheme in which a low-frequency excitation typically allows

for a rough resolution of the material profile, whereas an excitation with higher-frequency components fine-tunes the profile, and (c) a search-direction biasing scheme, whereby we seek to bias the λ-search directions by the μ-search directions, effectively forcing both parameters to increase simultaneously, during the early inversion iterations. The scheme is motivated by the physics of the problem, and is described by:

$$\mathbf{d}_k^\lambda \leftarrow \|\mathbf{d}_k^\lambda\| \left[W \frac{\mathbf{d}_k^\mu}{\|\mathbf{d}_k^\mu\|} + (1-W) \frac{\mathbf{d}_k^\lambda}{\|\mathbf{d}_k^\lambda\|} \right] \tag{17}$$

where a weighted average of *unit* λ- and μ-search directions are used for the evolution of λ.

5 NUMERICAL EXPERIMENTS

To test the proposed inversion scheme, we discuss next numerical experiments, involving arbitrarily heterogeneous hosts and synthetic data. The first example is a fictitious medium that has material properties varying smoothly with depth. We reduce the half-plane, through truncation, to a $45\text{m} \times 45\text{m}$ computational domain, surrounded on its sides and bottom by a 5m-thick PML, as shown in Fig. 5(a). The material interfaces were extended horizontally into

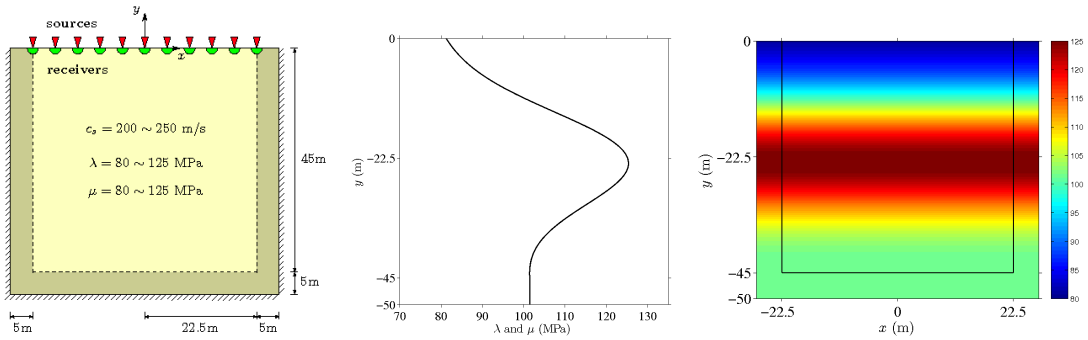

(a) Geometry (b) Cross-section (c) Target λ and μ

Figure 5: A PML-truncated semi-infinite domain in two dimensions

the PML, thereby, avoiding sudden material changes at the interface between the PML and the regular domain. We started the inversion process with a homogeneous profile that has both λ and μ set to 80 MPa. By applying a Gaussian pulse load with a maximum frequency of $f_r = 40$ Hz, we reconstructed the Lamé parameters shown in Fig. 6. Both Lamé parameters are satisfactorily inverted.

Example 2 involves a horizontally-layered medium with $\lambda(y) = \mu(y) = 80$, 101.25, and 125 MPa from top to bottom, as shown in Fig. 7(a). We use a source-frequency continuation scheme according to which a few time signals with different frequency content are used to probe the domain. We start the inversion process with a low-frequency source and feed the converged reconstructed λ and μ profiles as initial guesses to the problem excited with a higher-frequency source. Here, we considered four different Gaussian pulses with maximum frequencies of 10, 20, 30, and 40 Hz. Figure 8 shows the velocity profiles computed from the reconstructed Lamé parameter profiles. Both velocity profiles seem to be recovered quite satisfactorily.

The last example focuses on a layered medium with $\lambda(y) = \mu(y) = 320$, 500, 720 MPa from top to bottom and an embedded elliptic inclusion of 720 MPa in an effort to implicate arbitrary heterogeneity (Fig. 9). As in Example 2, we use a source-frequency continuation scheme with four distinct Gaussian pulses ($f_{\max} = 10$, 40, 80, and 120 Hz), to probe the

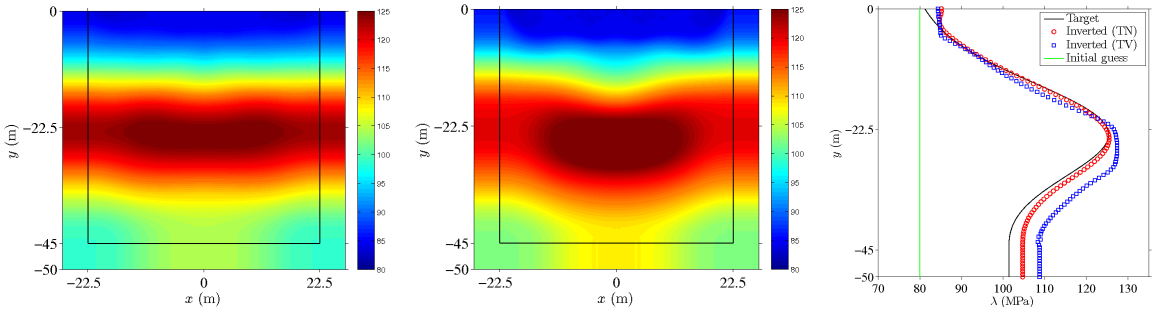

(a) λ (TN) (b) λ (TV) (c) λ at $x = 0$m

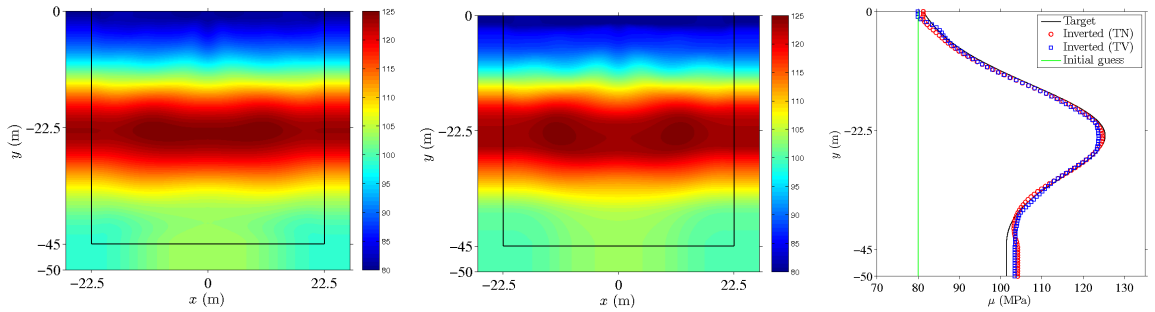

(d) μ (TN) (e) μ (TV) (f) μ at $x = 0$m

Figure 6: Simultaneous inversion for the Lamé parameters using TN and TV regularization

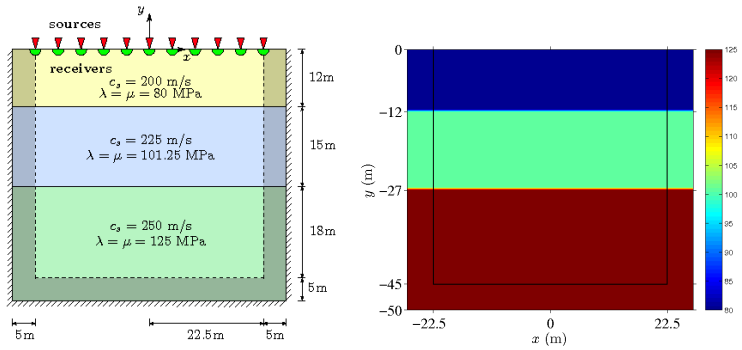

(a) Geometry (b) Target λ and μ

Figure 7: A PML-truncated horizontally-layered semi-infinite domain in two dimensions

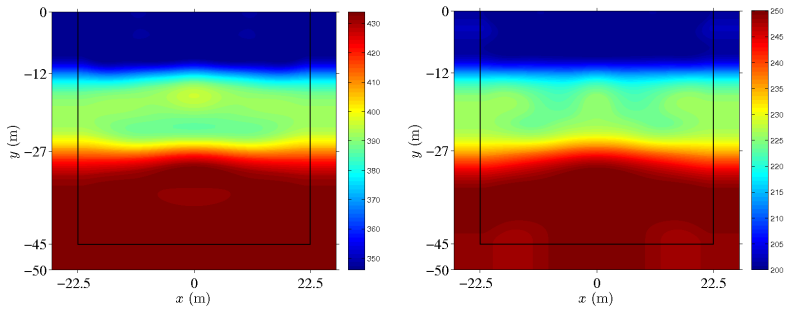

(a) c_p (m/s) (TN) (b) c_s (m/s) (TN)

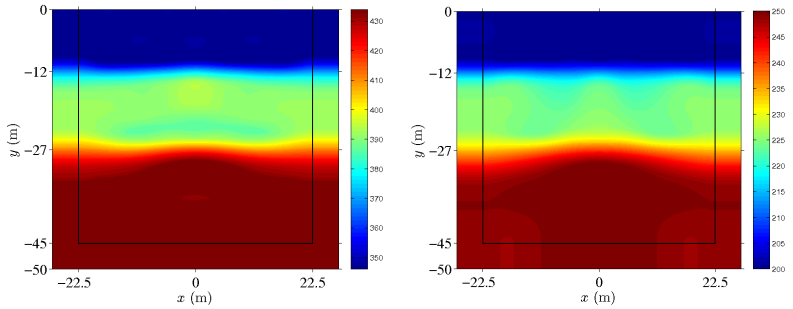

(c) c_p (m/s) (TV) (d) c_s (m/s) (TV)

Figure 8: Velocities computed from the reconstructed Lamé parameters

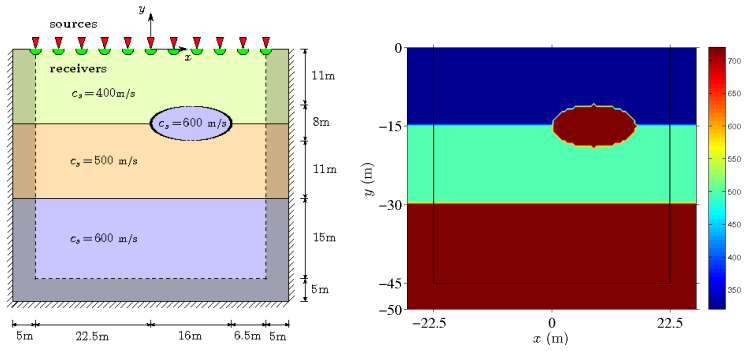

(a) Geometry (b) Target λ and μ

Figure 9: A PML-truncated layered semi-infinite domain with an elliptic inclusion

domain. Here we opted for using the TV regularization only. We initiated the inversion process with a homogeneous medium that has $\lambda = \mu = 310$ MPa. Figure 10 provides the velocity profiles computed from the reconstructed λ and μ. Once again, both velocity profiles seem to have been recovered with moderate success.

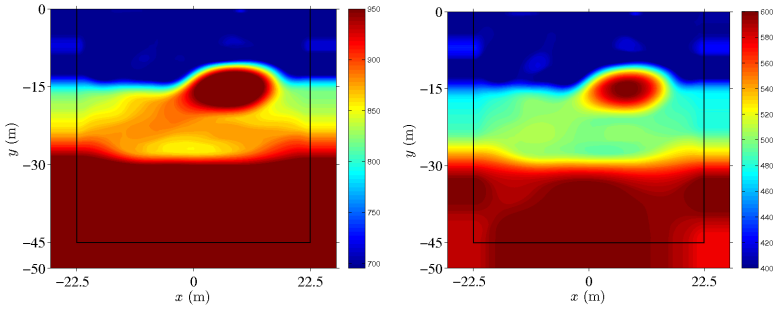

(a) c_p (m/s) (b) c_s (m/s)

Figure 10: Velocities computed from the reconstructed Lamé parameters

6 CONCLUSIONS

We discussed a full-waveform-based inversion methodology in PML-truncated elastic media, suitable for geotechnical site characterization purposes, implemented directly in the time-domain, using stress waves for probing, and driven by the measured response at receivers situated on the ground surface.

We adopted a PDE-constrained optimization approach, and discussed the implementation of the resulting first-order optimality conditions. These gave rise to: a) a state problem that was treated by the a new symmetric hybrid method developed for the forward wave simulation; b) an adjoint problem that was treated also with the hybrid method similarly to the state problem; and c) control problems that were used to update the material parameters. The continuation schemes we deployed assisted the optimizer in narrowing the initial feasibility space by presenting subsequent iterations with improved initial guesses. Though the presentation here is limited to geotechnical applications, the overall structure of the inversion scheme is modular and very flexible, and could be adopted as a solution approach for a broader class of inverse problems. Its performance can be improved by introducing a nonlinear iterative solver that would achieve convergence rates better than the conjugate gradient method used herein, possibly similar to what was proposed in [7].

We discussed our experience in reconstructing heterogeneous profiles involving smoothly-varying profiles, as well as layered systems, and layered media with embedded inclusions, in order to demonstrate the performance of the proposed inversion approach. Here, we described only the two-dimensional case, but the axisymmetric and three-dimensional cases follow directly.

REFERENCES

[1] W.C. Chew, Q.H. Liu, Perfectly matched layers for elastodynamics: a new absorbing boundary condition. *Journal of Computational Acoustics*, **4(4)**, 341–359, 1996.

[2] F. Collino, C. Tsogka, Application of the perfectly matched absorbing layer model to the linear elastodynamic problem in anisotropic heterogeneous media. *Geophysics*, **66(1)**, 294–307, 2001.

[3] U. Basu, A.K. Chopra, Perfectly matched layers for transient elastodynamics of unbounded domains. *Int. J. Numer. Meth. Engng.*, **59**, 1039–1074, 2004.

[4] D. Komatitsch, R. Martin, An unsplit convolutional perfectly matched layer improved at grazing incidence for the seismic wave equation. *Geophysics*, **72(5)**, SM155–SM167, 2007.

[5] K.C. Meza-Fajardo, A.S. Papageorgiou, A nonconvolutional, split-field, perfectly matched layer for wave propagation in isotropic and anisotropic elastic media: Stability analysis. *Bulletin of the Seismological Society of America*, **98(4)**, 1811–1836, 2008.

[6] S. Kucukcoban, L.F. Kallivokas, Mixed perfectly-matched-layers for direct transient analysis in 2D heterogeneous media. *Comput. Methods Appl. Mech. Engrg.*, **200(1-4)**, 57–76, 2011.

[7] I. Epanomeritakis, V. Akçelik, O. Ghattas, J. Bielak, A Newton-CG method for large-scale three-dimensional elastic full-waveform seismic inversion. *Inverse Problems*, **24(3)**, 34015–34040, 2008.

[8] J.W. Kang, L.F. Kallivokas, The inverse medium problem in heterogeneous PMLtruncated domains using scalar probing waves. *Computer Methods in Applied Mechanics and Engineering*, **200(1-4)**, 265–283, 2011.